

First in-beam PET measurement of $^{+}$ radioactivity induced by hard photon beams

This article has been downloaded from IOPscience. Please scroll down to see the full text article.

2007 Phys. Med. Biol. 52 N467

(<http://iopscience.iop.org/0031-9155/52/20/N01>)

View [the table of contents for this issue](#), or go to the [journal homepage](#) for more

Download details:

IP Address: 38.107.191.116

The article was downloaded on 02/09/2010 at 16:26

Please note that [terms and conditions apply](#).

NOTE

First in-beam PET measurement of β^+ radioactivity induced by hard photon beams

T Kluge¹, D Möckel¹, J Pawelke¹ and W Enghardt^{1,2}

¹ Division of Radiation Physics, Institute of Radiation Physics, Forschungszentrum Dresden-Rossendorf, PO Box 510119, 01314 Dresden, Germany

² Radiation Research in Oncology—OncoRay, University Hospital and Medical Faculty C G Carus, Technische Universität Dresden, Fetscherstraße 74, PO Box 86, 01307 Dresden, Germany

E-mail: t.kluge@fzd.de

Received 12 May 2007, in final form 27 July 2007

Published 1 October 2007

Online at stacks.iop.org/PMB/52/N467

Abstract

In this note, we present the first experimental results of in-beam PET measurements during high energy photon phantom irradiation. An inhomogeneous phantom was irradiated with pulsed 34 MV bremsstrahlung. The measurements have been conducted with a dedicated double head positron camera. A high material contrast could be achieved and furthermore production rates of ^{11}C and ^{15}O were derived from the time-dependent activity.

1. Introduction

Positron emission tomography (PET) is currently the only method for an *in situ* monitoring of heavy ion therapy (Enghardt *et al* 2004). In-beam PET has had a great impact on improving the precision of tumour irradiation since it is capable of detecting deviations from the planned dose delivery due to uncertainties in patient positioning and anatomy, equipment as well as deviations of the anticipated tumour response (Enghardt *et al* 2004, Brahme 2003). Additionally, washout of positron emitters affects their biological half-life, which can give information about biological transport processes (Hughes *et al* 1979, Fiedler *et al* 2006b).

It is therefore desirable to extend in-beam PET to radiotherapy with photon beams. In this case, positron emitters are produced by photonuclear (γ, n) reactions between photons and target nuclei (predominantly ^{14}N , ^{16}O , ^{12}C). These reactions show thresholds for photon energy values of 10.6 MeV, 15.7 MeV and 18.7 MeV, respectively (Chadwick *et al* 2000). Thus, for example in the case of intensity-modulated radiation therapy (IMRT) with hard photons ($E_{\text{max}} = 50$ MeV) as presented by Brahme *et al* (2001), the in-beam PET method could be feasible.

Recent research has been concentrated on the off-beam measurement of positron emitters produced via hard photon irradiation of phantoms as well as a leg of a pig (Möckel *et al* 2007, Janek *et al* 2006). Furthermore, Geant4 simulations have shown the feasibility of in-beam

PET (Müller and Enghardt 2006), predicting a dose-related activity for 50 MeV photon beams exceeding that of carbon ion beams (Fiedler *et al* 2006a). This note now presents for the first time experimental in-beam PET imaging data acquired with a dedicated detector system, continuing the work presented by Möckel *et al* (2007).

2. Materials and methods

2.1. Resume of the accelerator and phantoms

Irradiation with high energy photons was done at the electron linear accelerator for beams with high brilliance and low emittance (ELBE) at the Forschungszentrum Dresden-Rossendorf. The ELBE electron beam is predominantly used for generating secondary particles and radiation (Gabriel *et al* 2000). For the present work, the electron beam has been used to produce high energy bremsstrahlung of up to 34 MeV by irradiating an aluminium target of 18 μm thickness. Behind the aluminium target, the electron beam was steered into a beam dump by a dipole magnet, while the generated photon beam was used to irradiate the phantom.

In table 1 the range of possible beam parameters and those used in this experiment are listed. The beam current was chosen to produce a photon beam delivering to the phantom a dose rate of 4 Gy min^{-1} , which is a typical value for radiotherapy. As phantoms, blocks of the size 10 cm \times 10 cm \times 20 cm were used, with the long edge oriented parallel to the beam axis. The blocks consisted of 1 cm thick slabs of polymethyl methacrylate (PMMA), polyethylene (PE) or tissue equivalent material, stacked in an acrylic container. In table 2 relevant physical properties of the used materials are listed.

The mean dose rate was determined prior to the phantom irradiation by a short irradiation of an equally shaped block of PMMA equipped with intrinsic BeO dosimeters, as already

Table 1. Parameters of the ELBE electron beam (feasible values and values used in the experiments).

Parameter	Feasible value	Used value
Electron energy	12, . . . , 40 MeV	34 MeV
Beam current	$\leq 200 \mu\text{A}$	72 μA
Micro pulse duration	2 ps	2 ps
Micro pulse frequency	$26/2^n$ MHz, $n = 0, 1, \dots, 8$, 260 MHz	13 MHz
Macro pulse duration	0.1, . . . , 40 ms and cw ^a	36 ms
Macro pulse frequency	1, . . . , 25 Hz	8.3 Hz

^a Continuous wave.

Table 2. Physical density ρ , carbon density c_C , oxygen density c_O and the linear attenuation coefficient of 511 keV photons μ (Berger *et al* 2005) for materials that were used in the phantom. The designations of the Gammex materials are given in the brackets.

Material	ρ (g cm^{-3})	c_C (10^{22} cm^{-3})	c_O (10^{22} cm^{-3})	μ (cm^{-1})
1 PMMA	1.19	3.58	1.43	0.112
2 Lung1 ^a (LN300 RMI 455)	0.30	0.89	0.20	0.043
3 Lung2 ^a (LN450)	0.45	1.34	0.31	0.052
4 PE	0.93	4.00	0.00	0.093
5 Adipose ^a (AP6 RMI 453)	0.92	3.34	0.56	0.089
6 Bone ^a (CB2-30% CaCO_3)	1.34	3.59	1.29	0.121

^a Gammex Inc., Middleton, WI, USA.

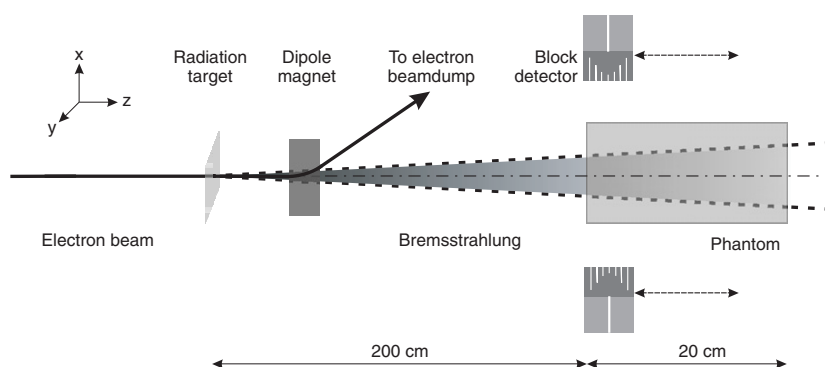


Figure 1. Schematic experimental setup, showing the bremsstrahlung production in the aluminium converter target and electron beam deflection by a dipole magnet. The activity produced in the phantom is measured by two BGO block detectors operating in the coincidence mode. To cover the whole phantom, they are continuously moved back and forth. The drawing is not to scale.

described by Möckel *et al* (2007), and corresponds to the dose measured at the maximum of the build-up region related to the irradiation time.

ELBE was operated in macro pulse mode with 84 ms pause between beam delivery, since the common photomultiplier-based photon detectors are saturated during the beam pulses, causing usually a break-down of the voltage divider, by photons originating mainly from positron–electron annihilation and scattering of bremsstrahlung in the phantom (Müller and Enghardt 2006, Brahme 2003). This allowed the detectors to recover, leaving an effective time of about 75 ms for the measurement during macro pulse pauses.

2.2. The in-beam detection system

The detector system used to measure the produced β^+ activity resembles a basic double head positron camera, operated in list mode. This allows only for two-dimensional imaging, since there is no spatial resolution along the detector connecting line. The basic experimental setup is depicted in figure 1.

As detector heads, two commercially available ECAT EXACT block detectors (Siemens, Erlangen, Germany) are used. They each consist of a 5.4 cm × 5.4 cm × 2.0 cm bismuth germinate (BGO) scintillator crystal. This is divided into 64 separate crystals by 7 × 7 slittings of different depths (Casey and Nutt 1986). This modulates the spatial distribution of the scintillation light in such a manner that the location of the incident photon can be determined by computing the barycentre of the four photomultiplier charge outputs. The incident photon energy is proportional to the sum of the photomultiplier charge outputs. The photomultiplier signals of each detector are processed by a preamplifier, which splits each signal into a shaped energy signal, having a nearly charge proportional voltage amplitude, and a fast timing signal, having a rise time of only about 2 ns. Additionally, the four timing signals of each detector are summed up by an analog adder. After being digitized by a constant fraction discriminator (CF8000, ORTEC), those summed timing signals serve as start and stop signals for a time-to-amplitude converter with a built-in single channel analyser (TAC/SCA 567, ORTEC). The SCA output then triggers the data acquisition.

To expand the field-of-view (FOV), the detectors are each mounted on a motion axis, allowing a synchronous movement of approximately 35 cm parallel to the beam direction at a speed of about 1.25 cm s⁻¹. While the phantom is being scanned continuously, data are taken by means of two National Instruments NI6143 PCI-boards connected to an industrial standard

personal computer running LabView under Microsoft Windows XP. The data acquisition system is capable of recording up to 250000 events s^{-1} in list mode. On each trigger event, the energy signals from both detectors and the TAC signal are converted to 16 bit digital values and latched in the on-board buffer until they are block-transferred to a hard disk at the end of each scan.

For an accurate reconstruction of the phantom activity, several corrections had to be applied to the raw data: (1) detector normalization: the varying sensitivity for annihilation photon detection over the detector cross section had to be normalized for all $64 \times 64 = 4096$ possible crystal combinations. For that, a ^{18}F β^+ radioactive flat source with a known activity concentration has been measured and the sensitivity for each single crystal pair was determined. (2) Attenuation correction: since acquisition was done in list mode, for each coincidence the line of response (LOR) and a correction factor f could be calculated. Those factors are obtained through $f = \prod_i \exp(\mu_i x_i)$ where μ_i is the linear absorption coefficient and x_i is the length of the LOR in the medium indexed by i . For the reconstruction each event was then weighted with its corresponding correction factor. (3) Random and scattered coincidences correction: all events with a photon energy outside the 511 keV full energy peak and a coincidence time outside the prompt peak of the coincidence time curve were rejected. Additionally, linear tail fitting was applied to the reconstructed data. For that, a linear function has been fitted into the scatter and random tails outside the phantom region and are subtracted from the reconstruction (Bailey *et al* 2005). (4) Correction for detector dead time: the dead time fraction could not be determined directly since the unaffected singles count rate was not recorded. Therefore, the time development of activity in the PE slabs was analysed. The difference between the measured activity and activity A expected from $A(t) = P_{^{11}\text{C}}[1 - \exp(-\lambda_{^{11}\text{C}} t)]$, where t is the irradiation time, $\lambda_{^{11}\text{C}}$ is the ^{11}C decay constant and $P_{^{11}\text{C}}$ is the ^{11}C production rate was computed and considered to be solely due to dead time. Subsequently, the measured activities in the remaining slabs were corrected with this dead time fraction. By doing so, the dead time fraction is assumed to be constant over the phantom volume. This is a reasonable approximation, since the single count rate is almost spatially constant.

3. Results

By means of in-beam PET the spatial distribution of positron emitters produced during high energy photon irradiation was imaged as presented in figure 2. The figure displays the experimentally obtained activity in each pixel, averaged over the phantom width (x -dimension, see figure 1) and integrated over the measurement duration of 80 min. The results show a significant activity contrast between all materials, based on their carbon and oxygen concentration. Only in PMMA and bone those concentrations are very similar (c_{C} and c_{O} varying less than 10%), resulting in a low activity contrast.

Activity originating both from ^{15}O and ^{11}C decay is contributing to the measured activity, as validated by figure 3. The figure sets in contrast the integrated activity density for a short acquisition time (integrating the activity over the first 10 min of irradiation) and a long acquisition time (80 min). For comparison, the expected values are also shown. They were computed by integrating the activity density

$$a = p_{^{11}\text{C}}[1 - \exp(-\lambda_{^{11}\text{C}} t)] + p_{^{15}\text{O}}[1 - \exp(-\lambda_{^{15}\text{O}} t)] \quad (1)$$

over time, with $\lambda_{^{11}\text{C}} = 0.57 \times 10^{-3} \text{ s}^{-1}$ and $\lambda_{^{15}\text{O}} = 5.67 \times 10^{-3} \text{ s}^{-1}$ being the ^{11}C and ^{15}O decay constants, and using

$$p_i = c_i \int_0^{E_{\text{max}}} v(E) \sigma_i(E) dE \equiv c_i \Sigma_i \quad (2)$$

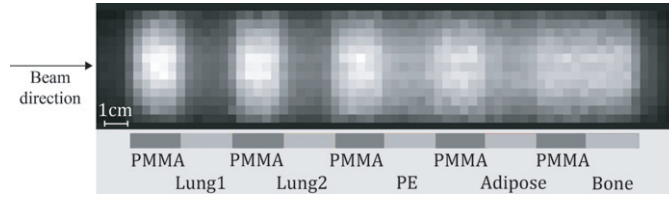


Figure 2. Two-dimensional distribution of integrated activity density averaged over the phantom width. (Linear greyscale, white corresponds to the maximum value.)

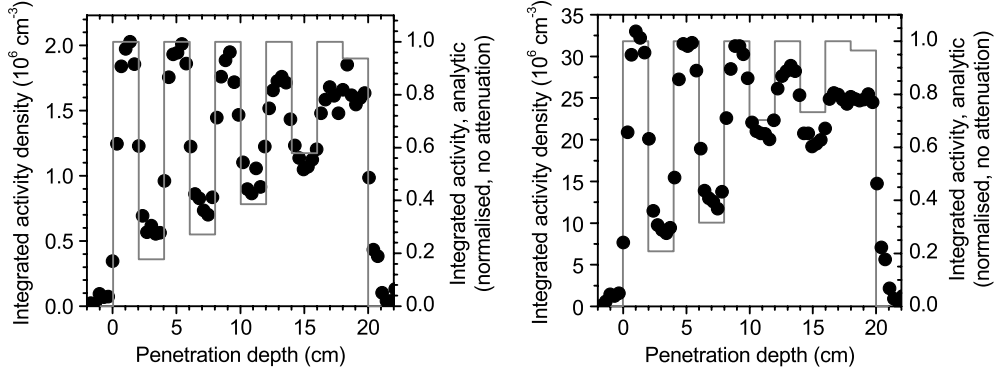


Figure 3. Depth profile of integrated activity after 10 min (left) and 80 min (right) of irradiation at a dose rate of 4 Gy min^{-1} . Shown is the mean value of the projection on the beam axis of the part depicted in figure 2 (dots) and the analytic values (solid line). Please note that the integrated activity is dimensionless.

where σ_i are the cross section values for the corresponding (γ, n) reaction obtained from Chadwick *et al* (2000), $\nu(E)$ is the spectral photon beam flux obtained from an analytical expression (Jackson (1982), p 853), and Σ_i is the production rate density per target atom of the species indexed by i .

Due to the longer half-life of ^{11}C (20.4 min) compared to ^{15}O (2.0 min), at a short measurement time the activity mostly originates from ^{15}O decay while for long measurement times it becomes more influenced by ^{11}C activity. Thus, the material contrasts change over time, dependent on the $c_{\text{C}}/c_{\text{O}}$ ratio. This effect is clearly visible for the adipose tissue equivalent material and PE, where the PE activation builds up slower due to the absence of ^{16}O .

By plotting the measured activity as a function of time t , as displayed in figure 4, the production rates of ^{11}C and ^{15}O could be inferred experimentally. A fit with the exponential growth function (equation (1)) yields the production rates p listed in table 3. Conclusions can be drawn on the ratio of carbon and oxygen concentrations by

$$\frac{c_{\text{C}}}{c_{\text{O}}} = \frac{p_{^{11}\text{C}}}{p_{^{15}\text{O}}} \cdot \frac{\Sigma_{^{15}\text{O}}}{\Sigma_{^{11}\text{C}}}. \quad (3)$$

The experimentally obtained $c_{\text{C}}/c_{\text{O}}$ fractions in comparison to the values provided by the manufacturer are also given in table 3. They show a rather large error margin, not allowing us to differentiate between Lung2 and Lung1 or Adipose, for example. However, the experimentally obtained values coincide with those given from the manufacturer within experimental accuracy excepting PE, whose deviation can be explained with the recovery

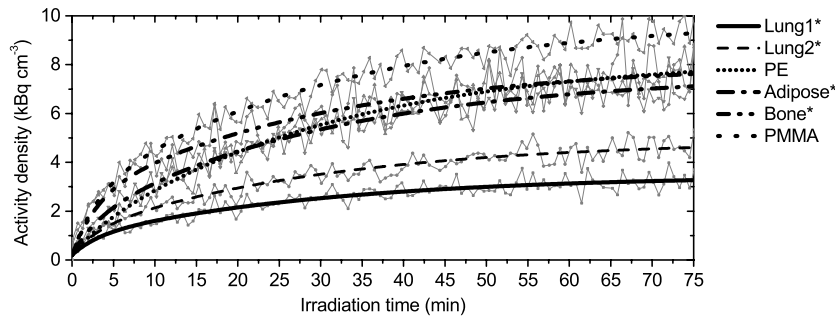


Figure 4. Activity density in dependence on irradiation time at a dose rate of 4 Gy min^{-1} for different materials as well as the corresponding curve fits (bold) of equation (1) to the experimental data.

Table 3. Production rate density p of ^{11}C and ^{15}O at a dose rate of 4 Gy min^{-1} as obtained by curve fitting equation (1) to experimental data of figure 4, and carbon and oxygen concentration c .

Material	$p_{^{11}\text{C}}$ ($\text{s}^{-1} \text{ cm}^{-3}$)	$p_{^{15}\text{O}}$ ($\text{s}^{-1} \text{ cm}^{-3}$)	$c_{\text{C}}/c_{\text{O}}$	
			Experimental	Manufacturer
PMMA ^a	7065 ± 320	2666 ± 200	2.65 ± 0.32	2.50
Lung1	2602 ± 120	648 ± 83	3.87 ± 0.67	4.45
Lung2	3870 ± 140	790 ± 100	4.72 ± 0.76	4.32
PE ^b	7690 ± 210	260 ± 140	28.5 ± 16.1	∞
Adipose	6240 ± 210	1010 ± 150	5.95 ± 1.09	5.96
Bone	5710 ± 310	1860 ± 220	2.96 ± 0.51	2.78

^a Second PMMA slab.

^b PE was used for dead time correction.

effect. This means that the reconstructed activity is deteriorated by the finite width of the detector response function, which is of the same magnitude as the phantom slabs.

4. Conclusion and outlook

In this work, we have presented our first experimental results of in-beam PET measurements during the irradiation with a pulsed hard photon beam. The induced ^{11}C and ^{15}O activity was quantified by a dedicated double-head photon camera, showing a high contrast for materials differing in carbon or oxygen concentration more than 10%. Compared to prior off-beam measurements (Möckel *et al* 2007) the contrast is considerably improved, especially between materials with comparable carbon but differing oxygen concentration (e.g. PMMA and PE).

Based on the experimental results so far it can be stated that in-beam PET is in principle capable of mapping anatomical structures during patient irradiation, because the ratio of carbon and oxygen concentrations can be computed from the ratio of ^{11}C and ^{15}O activities. Especially the oxygen activity is only reasonably measurable with in-beam PET due to its short half-life. Thus, this method could be used as a valuable tool for quality assurance of hard photon tumour irradiation since patient positioning, beam delivery and treatment planning can be controlled.

An upcoming paper will address the comparison of in-beam and off-beam data in more detail and present data on the dose-related activity concentration. This is needed to correlate the measured activity to the applied dose and thus for a control of dose delivery.

Acknowledgments

The authors would like to thank the ELBE-crew for support in the realization of the experiments. This work was funded by the European Commission under the 6th Research Framework Programme (Contract no. LSHC-CT-2004-505785). This publication does not necessarily reflect the view of the EC, nor is it liable for any use that may be made of the information contained herein. The information in this document is provided as is and no guarantee or warranty is given that the information is fit for any particular purpose. The reader thereof uses the information at its sole risk and liability.

References

- Bailey D L, Townsend D W, Valk P E and Maisey M N (ed) 2005 *Positron Emission Tomography* (London: Springer Verlag)
- Berger M J, Hubbell J H, Seltzer S M, Chang J, Coursey J S, Sukumar R and Zucker D S 2005 *XCOM: Photon Cross Sections Database (version 1.3)* (Gaithersburg, MD: National Institute of Standards and Technology) <http://physics.nist.gov/xcom>
- Brahme A 2003 Biologically optimized 3-dimensional *in vivo* predictive assay-based radiation therapy using positron emission tomography-computerized tomography imaging *Acta Oncol.* **42** 123–36
- Brahme A, Nilsson J and Belkic D 2001 Biologically optimized radiation therapy *Acta Oncol.* **40** 725–34
- Casey M E and Nutt R 1986 A multi-crystal two dimensional BGO detector system for positron emission tomography *IEEE Trans. Nucl. Sci.* **33** 460
- Chadwick M B *et al* 2000 *IAEA Photonuclear Data Library* (Vienna, Austria: International Atomic Energy Agency) <http://www-nds.iaea.org/photonuclear>
- Enghardt W, Crespo P, Fiedler F, Hinz R, Parodi K, Pawelke J and Pönisch F 2004 Charged hadron tumour therapy monitoring by means of PET *Nucl. Instrum. Methods A* **525** 284–8
- Fiedler F, Crespo P, Parodi K, Sellesk M and Enghardt W 2006a The feasibility of in-beam PET for therapeutic beams of ^3He *IEEE Trans. Nucl. Sci.* **53** 2252–9
- Fiedler F, Sellesk M and Enghardt W 2006b Washout studies performed via in-beam PET *IKH Ann. Rep.* **FZR-442** 61
- Gabriel F, Gippner P, Grosse E, Janssen D, Michel P, Prade H, Schamlott A, Seidel W, Wolf A and Wünsch R 2000 The Rossendorf radiation source ELBE and its FEL projects *Nucl. Instrum. Methods B* **161** 1143–7
- Hughes W L, Nussbaum G H, Connolly R, Emami B and Reilly P 1979 Tissue perfusion rate determined from the decay of oxygen-15 activity after photon activation in situ *Science* **204** 1215–7
- Jackson J D 1982 *Klassische Elektrodynamik* (Berlin: de Gruyter)
- Janek S, Svensson R and Brahme A 2006 Development of dose delivery verification by PET imaging of photonuclear reactions following high energy photon therapy *Phys. Med. Biol.* **51** 5769–83
- Möckel D, Müller H, Pawelke J, Sommer M, Will E and Enghardt W 2007 Quantification of β^+ activity generated by hard photons by means of PET *Phys. Med. Biol.* **52** 2515–30
- Müller H and Enghardt W 2006 In-beam PET at high-energy photon beams: a feasibility study *Phys. Med. Biol.* **51** 1779–89